A dynamical envelope model for vibratory gyroscopes

authored by **M. Egretzberger and A. Kugi**

and published in *Microsystem Technologies*.

Automation and Control Institute (ACIN)
Vienna University of Technology
Gusshausstrasse 27-29/E376
1040 Vienna, Austria

Internet: www.acin.tuwien.ac.at
E-mail: office@acin.tuwien.ac.at
Phone: +43 1 58801 37601
Fax: +43 1 58801 37699

Microsystem Technologies manuscript No.
(will be inserted by the editor)

A dynamical envelope model for vibratory gyroscopes

Markus Egretzberger · **Andreas Kugi**

Received: date / Accepted: date

Abstract In this contribution, a method will be presented to derive an envelope model for vibratory gyroscopes capturing the essential ”slow” dynamics (envelope) of the system. The methodology will be exemplarily carried out for a capacitive gyroscope with electrostatic actuators and sensors. The resulting envelope model can be utilized for both transient and steady state simulations with the advantage of a significantly increased simulation speed. Especially for the sensor design and optimization, where usually very complex mathematical models are used, efficient steady state simulations are of certain interest. Another great advantage of this approach is that the steady state solutions in terms of the envelope model are constant. Thus, for the controller design, a linearization of the nonlinear envelope model around the steady state solution yields a linear time-invariant system allowing for the application of the powerful methods known from linear control theory.

1 Introduction

Vibratory micro electromechanical gyroscopes are typically driven by a primary oscillator. This primary oscillation is usually excited close to the resonance frequency in order to achieve maximum amplitudes. Similar to many electronic circuits, in particular in information technology, the wanted signal is modulated in a high-frequency carrier signal. Thus, the rate of change of the wanted signals is several orders of magnitude slower than the carrier frequency. In the case of the vibratory micro electromechanical gyroscopes under consideration an external angular rate causes a secondary oscillation with an amplitude proportional to the angular rate component about the sensitive axis exploiting the Coriolis effect. The output signal of the sensor (i.e., the angular rate) is obtained by an appropriate demodulation of the secondary oscillation signal. In order to provide a linear sensor behavior with maximum sensitivity the frequency and amplitude of the primary oscillation have to be controlled. Therefore, control circuits are used with a functionality similar to those of phase-locked loop and automatic gain-control circuits. Furthermore, micro electromechanical sensors are subject to large quadrature errors due to limitations in the fabrication process. These quadrature errors typically are due to a mechanical unbalance which causes a coupling between the primary and secondary oscillation even without an applied external angular rate. This quadrature signal can be usually separated from the angular rate signal after the demodulation of the secondary oscillation. In order to avoid a drift of the output signal, e.g., over the temperature, due to demodulation errors the mechanical unbalance has to be actively compensated. Therefore, an additional actuation of the secondary oscillator has to be provided such that a controller can be implemented to suppress the unwanted quadrature signal. In this context, many articles dealing with the control of vibratory gyroscopes can be found in the literature, see, e.g., Bernstein et al (1993), Bhave et al (2003), Günthner et al (2005), Kuisma et al (1997), Loveday and Rogers (2002), Maenaka et al (1996), Sassen et al (2000). In addition to the above mentioned control tasks necessary for the basic operation of micro electromechanical gyroscopes, force-feedback control and frequency control of the secondary resonance frequency are often used to further enhance the sensor performance. All of the mentioned control loops have in common that the relevant closed-loop dynamics lie within the frequency range of the envelope of the signal rather than in the frequency range of the carrier signal itself. In particular from a system analysis and controller

M. Egretzberger · A. Kugi
Automation and Control Institute (ACIN)
Vienna University of Technology
Gusshausstr. 27-29, 1040 Wien, Austria
E-mail: egretzberger@acin.tuwien.ac.at, kugi@acin.tuwien.ac.at

Pre-print version of the article: M. Egretzberger and A. Kugi, “A dynamical envelope model for vibratory gyroscopes”, *Microsystem Technologies*, vol. 16, pp. 777–786, 2010. DOI: 10.1007/s00542-009-0979-y

design point of view, this motivates to derive a more comprehensive mathematical model which solely captures the essential ”slow” dynamics (envelope) of the system. In this context see also Kanso et al (2004).

In this contribution, the method for the derivation of an envelope model introduced by Egretzberger and Kugi (2009) will be picked up and expanded to include a simplified model suitable for the systematic controller design. The methodology will be exemplarily carried out for a capacitive micro electromechanical gyroscope. This paper is organized as follows. In Sect. 2 the specific capacitive gyroscope is discussed, which will serve as a practical example for the theory being presented. A mathematical model for the gyroscope under consideration is given as a starting point for the derivation of an envelope model in Sect. 3. Subsequently, Sect. 4 and Sect. 5 are focused on the application of the envelope model in terms of calculating the steady state and transient response to an angular rate or mechanical unbalance. In order to provide a suitable model for a systematic controller design on the basis of the ”slow” system dynamics, however, it is reasonable to make some more efforts in order reduction and further simplification of the envelope model. Therefore, Sect. 6 is concerned with the derivation of a simplified two modes envelope model. Finally, the working principle and the typical control tasks of vibratory gyroscopes are discussed by means of the simplified envelope model. The work is concluded by a short summary.

2 A capacitive gyroscope

The micro electromechanical device that will be considered within this paper is a gyroscope consisting of a plane symmetric silicon structure operating with an in-plane primary mode, excited by capacitive comb actuators, and an out-of-plane secondary mode with capacitive parallel plate sensors. Most capacitive gyroscopes found in the literature are driven by electrostatic comb actuators bringing about the advantage of a high actuation force and little required space. They are found in linear oscillating as well as in rotating designs, see, e.g., Alper and Akin (2001), Bhave et al (2003), Braxmaier et al (2003), Piyabongkarn et al (2005), Seshia et al (2002) and Juneau et al (1997), respectively. For the same reason the read-out of the secondary oscillation is preferably also realized by means of comb sensors. Obviously, comb sensors require the secondary mode to be also an in-plane oscillation as it is the case for the designs presented by Alper and Akin (2001), Braxmaier et al (2003), Piyabongkarn et al (2005), Seshia et al (2002). If the secondary mode is an out-of-plane oscillation, parallel plate capacitors are utilized such that the movable electrode is part of the oscillating structure and the appropriate fixed electrode is mounted on the housing of the device, see, e.g., Günthner (2006).

Within the scope of this work several geometric designs deduced from the capacitive gyroscope presented by Günthner (2006) have been studied. The increasing complexity of the sensor design and the large variety of design modifications have given rise to the development of a software tool for the automatic generation of an analytical mathematical model for this type of capacitive gyroscopes. This software tool is capable of reading slightly refined geometric design data provided by CAD tools and converts the geometric information of the structure into functional elements necessary for the mathematical modeling of the gyroscope. A data interface is provided for a program package developed for the commercial computer algebra program MAPLE, which allows for the analytical modeling of the gyroscope and the subsequent export of a suitable model for the numeric simulation environment MATLAB/SIMULINK. The software tool is described in more detail by Mair et al (2009) and will be utilized in the present work for the derivation of the mathematical model.

At this point, let us restrict ourselves to one specific design which is an enhanced version of the gyroscope presented by Günthner (2006). This design is capable of both compensating the mechanical unbalance and tuning the eigenfrequency of the secondary mode. In this section, the working principle of the capacitive gyroscope will be explained and subsequently the appropriate mathematical model is derived.

2.1 Principle of operation

The capacitive gyroscope under consideration as depicted in Fig. 1 is an etched, plane silicon structure possessing two axes of symmetry. It consists of a rectangular fixed frame, which is rigidly mounted on the housing of the device, and two movable frames, one on the left and one on the right half of the sensor, which are flexibly connected to the fixed frame via elastic beams, the so-called drive beams. Moreover, two paddles are flexibly connected to each movable frame via torsion beams.

The comb actuators and comb sensors comprise electrodes residing on the fixed frame and their movable counterparts which are rigidly attached to the movable frames. The comb actuators allow for a harmonic excitation of the movable frames and the paddles in an anti-symmetric in-plane oscillation (primary mode). If an external angular rate is applied to the system the Coriolis force is coupling to the velocity of the movable frames and paddles causing an out-of-plane motion of these rigid body elements (secondary mode). The comb sensors provide the feedback signal for the amplitude control of the primary mode while the secondary mode is detected by means of four parallel plate capacitors with a fixed electrode placed on the housing above each

Pre-print version of the article: M. Egretzberger and A. Kugi, “A dynamical envelope model for vibratory gyroscopes”, *Microsystem Technologies*, vol. 16, pp. 777–786, 2010. DOI: 10.1007/s00542-009-0979-y
The content of this pre-print version is identical to the published paper but without the publisher's final layout or copy editing.

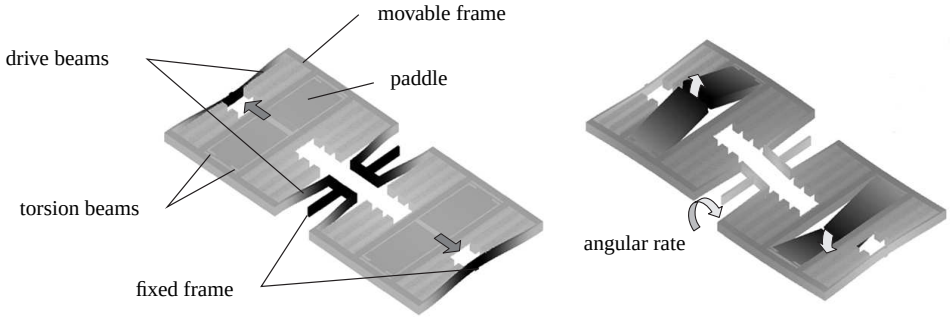

(a) Primary mode (b) Secondary mode

Fig. 1 Schematic representation of the capacitive gyroscope (a) primary mode and (b) secondary mode.

paddle. Furthermore, there are additional capacitive parallel plate actuators, each of which consisting of several fixed electrodes placed above the movable frame and the paddles. The mechanical unbalance which is coupling the primary and the secondary mode is due to a distortion of the rectangular shaped cross sections of the beam elements, in particular at the drive meanders. In the mathematical model derived below this effect will be accounted for by means of beam elements with rhomboid cross sections characterized by the so-called side wall angle ξ, see Merz et al (2007). All electrostatic actuators are assumed to be voltage controlled with a desired input voltage, see, e.g., Seeger and Boser (2003). The electrostatic sensors are realized by means of so-called charge amplifier circuits to convert the capacitance change into a proportional output voltage. These circuits are complemented by appropriate differential amplifiers in order to obtain applicable output signals for the detection of the primary and secondary mode.

2.2 Mathematical model

As described in Subsect. 2.1 the micro electromechanical device is composed of several components, i.e., the movable mechanical structure consisting of rigid elements (movable frame, paddle), elastic elements (beam structures) and the electrostatic actuators (comb and parallel plate capacitors). In a more general form, the capacitive gyroscope can be considered as a multi-body system made up of rigid and elastic bodies with external forces applied by the capacitive actuators. The equations of motion can be derived by means of Lagrange's formalism, e.g. by utilizing the software tool presented by Mair et al (2009). The resulting model is a system of non-linear ordinary differential equations of the form

$$\mathbf{M}(\mathbf{z})\,\ddot{\mathbf{z}} + \mathbf{C}(\mathbf{z},\dot{\mathbf{z}},\Omega)\,\dot{\mathbf{z}} + \mathbf{f}\big(\mathbf{z},\mathbf{u},\Omega,\dot{\Omega},\xi\big) = \mathbf{0} \tag{1a}$$

with the output

$$\mathbf{y} = \mathbf{h}(\mathbf{z}) \ , \tag{1b}$$

the vector of the generalized displacements $\mathbf{z}$, the externally applied angular rate Ω and the vector of input voltages $\mathbf{u}$ and output voltages $\mathbf{y}$. Note that $\mathbf{M}(\mathbf{z})$ is the positive definite inertia matrix, $\mathbf{C}(\mathbf{z},\dot{\mathbf{z}},\Omega)$ is the Coriolis matrix and the side wall angle ξ represents the mechanical unbalance of the gyroscope. Since the displacements $\mathbf{z}$ are small the autonomous mechanical system with $\Omega = 0$ and $\mathbf{u} = \mathbf{0}$ can be linearized around the equilibrium point $\mathbf{z} = \dot{\mathbf{z}} = \mathbf{0}$ and the eigenmodes and eigenvectors of the (decoupled) mechanical structure with $\xi = 0$ can be calculated. The state transformation $\mathbf{z} = \mathbf{T}\,\mathbf{q}$ with the regular matrix $\mathbf{T}$ containing the eigenvectors of the linearized autonomous system substituted in Eq. 1 yields a modal model which allows for a systematic order reduction. So far the system has been considered as a conservative system, i.e., without dissipative terms. Within the scope of this contribution a modal damping model will be used by adding the dissipative term $-\mathbf{D}\,\dot{\mathbf{q}}$ with a diagonal matrix $\mathbf{D}$. Due to the specific design of the gyroscope some further simplifications can be made. The structure is optimized to yield a maximum Coriolis effect while at the same time suppressing the inertia and centrifugal terms due to the external angular rate. In view of these assumptions all non-linear terms of the mechanical subsystem are neglected except for the Coriolis terms stemming from the external angular rate Ω. Then, the transformed (modal) system can be written in the form

$$\frac{\mathrm{d}}{\mathrm{d}t}\begin{bmatrix}\mathbf{q}\\ \mathbf{v}\end{bmatrix} = \begin{bmatrix}\mathbf{0} & \mathbf{I}\\ -\tilde{\mathbf{K}}(\xi) & -\tilde{\mathbf{D}}(\Omega)\end{bmatrix}\begin{bmatrix}\mathbf{q}\\ \mathbf{v}\end{bmatrix} - \begin{bmatrix}\mathbf{0}\\ \tilde{\mathbf{f}}(\mathbf{q},\mathbf{u})\end{bmatrix} \tag{2a}$$

with the output

$$\mathbf{y} = \tilde{\mathbf{h}}(\mathbf{q}) \ , \tag{2b}$$

the vectors of the states $\mathbf{q},\mathbf{v} \in \mathbb{R}^n$, the vector of the input voltages $\mathbf{u} \in \mathbb{R}^m$ and the output voltages $\mathbf{y} \in \mathbb{R}^p$. Thereby, $\tilde{\mathbf{K}}(\xi)$ denotes the stiffness matrix of the mechanical system depending on the side wall angle ξ, the matrix $\tilde{\mathbf{D}}(\Omega)$ contains the dissipative terms and the Coriolis terms due to the external angular rate Ω and the vector $\tilde{\mathbf{f}}(\mathbf{q},\mathbf{u})$ comprises the

Pre-print version of the article: M. Egretzberger and A. Kugi, "A dynamical envelope model for vibratory gyroscopes", *Microsystem Technologies*, vol. 16, pp. 777–786, 2010. DOI: 10.1007/s00542-009-0979-y

non-linear electromechanical coupling terms due to the capacitive actuation.

In the case of the capacitive gyroscope from Fig. 1 the input vector $\mathbf{u}$ consists of m input voltages, namely the drive voltage u_D at the comb actuators and the compensation voltages $u_{C,j}$, $j = 1,\ldots,m-1$ applied to the parallel plate actuators for suppressing the mechanical unbalance due to the side wall angle ξ and for tuning the eigenfrequency of the secondary mode. The exact number of compensation voltages is not specified at this stage, since it varies for each specific design under consideration. For the subsequent calculations a numerical model reduced to $n = 8$ modes will be used. Thereby, the fundamental modes of the gyroscope, i.e., the primary and secondary mode, coincide with the second and third eigenmode q_2 and q_3 of the eight modes model, respectively. Finally, the output vector $\mathbf{y} = [y_P, y_S]^{\mathrm{T}}$ consists of the primary and secondary detection voltages y_P and y_S provided by the capacitive comb sensors and parallel plate sensors, respectively. The corresponding charge amplifier is supplied by the read-out voltage u_{RO} which will be considered as a constant parameter.

3 Envelope model

Now, the system Eq. 2 is excited by the harmonic drive voltage u_D in order to operate the system at the eigenfrequency of the primary mode. In many cases the relevant dynamics lie within the frequency range of the envelope of the signal rather than in the frequency range of the harmonically oscillating signal itself. This leads to the idea of developing a model that is described by the Fourier coefficients of the appropriate harmonic signals, see, e.g., Caliskan et al (1996).

Starting from the general mathematical model Eq. 2 a Fourier transformation $\mathbf{q} = \mathbf{Q}^{\mathrm{T}}\mathbf{w}$, $\mathbf{v} = \mathbf{V}^{\mathrm{T}}\mathbf{w}$, $\mathbf{u} = \mathbf{U}^{\mathrm{T}}\mathbf{w}$ and $\mathbf{y} = \mathbf{Y}^{\mathrm{T}}\mathbf{w}$ is performed with the Fourier coefficient matrices $\mathbf{Q},\mathbf{V} \in \mathbb{R}^{2r+1\times n}$, $\mathbf{U} \in \mathbb{R}^{2r+1\times m}$ and $\mathbf{Y} \in \mathbb{R}^{2r+1\times p}$ of the form

$$\mathbf{Q} = \begin{bmatrix} Q_{1,0} & \cdots & Q_{n,0} \\ Q_{1,S} & & Q_{n,S} \\ Q_{1,C} & & Q_{n,C} \\ \vdots & \ddots & \vdots \\ Q_{1,rS} & & Q_{n,rS} \\ Q_{1,rC} & \cdots & Q_{n,rC} \end{bmatrix}, \quad \mathbf{V} = \begin{bmatrix} V_{1,0} & \cdots & V_{n,0} \\ V_{1,S} & & V_{n,S} \\ V_{1,C} & & V_{n,C} \\ \vdots & \ddots & \vdots \\ V_{1,rS} & & V_{n,rS} \\ V_{1,rC} & \cdots & V_{n,rC} \end{bmatrix},$$

$$\mathbf{U} = \begin{bmatrix} U_{1,0} & \cdots & U_{m,0} \\ U_{1,S} & & U_{m,S} \\ U_{1,C} & & U_{m,C} \\ \vdots & \ddots & \vdots \\ U_{1,rS} & & U_{m,rS} \\ U_{1,rC} & \cdots & U_{m,rC} \end{bmatrix}, \quad \mathbf{Y} = \begin{bmatrix} Y_{1,0} & \cdots & Y_{p,0} \\ Y_{1,S} & & Y_{p,S} \\ Y_{1,C} & & Y_{p,C} \\ \vdots & \ddots & \vdots \\ Y_{1,rS} & & Y_{p,rS} \\ Y_{1,rC} & \cdots & Y_{p,rC} \end{bmatrix} \tag{3}$$

and the Fourier basis vector $\mathbf{w} \in \mathbb{R}^{2r+1}$

$$\mathbf{w} = \left[1,\, \sin(\varphi),\, \cos(\varphi),\, \ldots,\, \sin(r\varphi),\, \cos(r\varphi)\right]^{\mathrm{T}},$$

with the phase φ. The Fourier basis vector $\mathbf{w}$ satisfies the differential equation $\dot{\mathbf{w}} = \boldsymbol{\Omega}\,\mathbf{w}$ with the phase velocity matrix

$$\boldsymbol{\Omega} = \begin{bmatrix} 0 & 0 & 0 & \cdots & 0 & 0 \\ 0 & 0 & \omega & & 0 & 0 \\ 0 & -\omega & 0 & & 0 & 0 \\ \vdots & & & \ddots & & \vdots \\ 0 & 0 & 0 & & 0 & r\omega \\ 0 & 0 & 0 & \cdots & -r\omega & 0 \end{bmatrix}$$

and the phase velocity $\omega = \dot{\varphi}$ of the fundamental oscillation. If it is assumed that the non-linear terms in Eq. 2 can be written in the form $\tilde{\mathbf{f}}(\mathbf{q},\mathbf{u}) = \tilde{\mathbf{F}}^{\mathrm{T}}(\mathbf{Q},\mathbf{U})\,\mathbf{w}$ and $\tilde{\mathbf{h}}(\mathbf{q}) = \tilde{\mathbf{H}}^{\mathrm{T}}(\mathbf{Q})\,\mathbf{w}$, the above Fourier transform substituted in Eq. 2 yields the matrix-valued differential equations

$$\frac{\mathrm{d}}{\mathrm{d}t}\begin{bmatrix}\mathbf{Q}^{\mathrm{T}} \\ \mathbf{V}^{\mathrm{T}}\end{bmatrix} = \begin{bmatrix}\mathbf{0} & \mathbf{I} \\ -\tilde{\mathbf{K}}(\xi) & -\tilde{\mathbf{D}}(\Omega)\end{bmatrix}\begin{bmatrix}\mathbf{Q}^{\mathrm{T}} \\ \mathbf{V}^{\mathrm{T}}\end{bmatrix} - \begin{bmatrix}\mathbf{0} \\ \tilde{\mathbf{F}}^{\mathrm{T}}(\mathbf{Q},\mathbf{U})\end{bmatrix} - \begin{bmatrix}\mathbf{Q}^{\mathrm{T}} \\ \mathbf{V}^{\mathrm{T}}\end{bmatrix}\boldsymbol{\Omega} \tag{4a}$$

with the output

$$\mathbf{Y}^{\mathrm{T}} = \tilde{\mathbf{H}}^{\mathrm{T}}(\mathbf{Q})\ . \tag{4b}$$

Since in general the Fourier transform of the non-linear terms cannot be calculated analytically the discrete Fourier transform will be utilized similarly to the approach proposed by Feldman and Roychowdhury (1996) for the computation of circuit waveform envelopes. For this, a discretization of one period $T = 2\pi/\omega$ of the fundamental oscillation with N equidistant time steps is performed. If the discretized state vectors $\mathbf{q}_k$ and input vectors $\mathbf{u}_k$ for the time steps $k = 1,\ldots,N$ are merged into a matrix

$$\hat{\mathbf{q}} = [\hat{\mathbf{q}}_1,\ldots,\hat{\mathbf{q}}_N]^{\mathrm{T}} \quad \text{and} \quad \hat{\mathbf{u}} = [\hat{\mathbf{u}}_1,\ldots,\hat{\mathbf{u}}_N]^{\mathrm{T}}\ ,$$

respectively, the inverse discrete Fourier transform with real coefficients directly relates $\hat{\mathbf{q}}$ and $\hat{\mathbf{u}}$ with $\mathbf{Q}$ and $\mathbf{U}$ in the form

$$\hat{\mathbf{q}} = \frac{1}{N}\boldsymbol{\Lambda}\,\mathbf{Q}\ ,\quad \hat{\mathbf{u}} = \frac{1}{N}\boldsymbol{\Lambda}\,\mathbf{U}$$

with the transformation matrix

$$\boldsymbol{\Lambda} = \begin{bmatrix} 1 & 0 & 1 & \ldots & 0 & 1 \\ \vdots & & & \ddots & & \vdots \\ 1 & \sin(a_k) & \cos(a_k) & \ldots & \sin(ra_k) & \cos(ra_k) \\ \vdots & & & \ddots & & \vdots \\ 1 & \sin(a_N) & \cos(a_N) & \ldots & \sin(ra_N) & \cos(ra_N) \end{bmatrix},$$

$a_k = 2\pi(k-1)/N\ ,\quad k = 2,\ldots,N\ .$

If $N > 2r$, i.e., the sampling theorem is satisfied, the transformation matrix $\boldsymbol{\Lambda}$ has $2r+1$ linearly independent rows. Now the non-linear terms in Eq. 2 can be calculated for every time step $k = 1,\ldots,N$ in the form $\hat{\mathbf{f}}_k = \tilde{\mathbf{f}}(\hat{\mathbf{q}}_k,\hat{\mathbf{u}}_k)$ and

Pre-print version of the article: M. Egretzberger and A. Kugi, "A dynamical envelope model for vibratory gyroscopes", *Microsystem Technologies*, vol. 16, pp. 777–786, 2010. DOI: 10.1007/s00542-009-0979-y

$\hat{\mathbf{h}}_k = \tilde{\mathbf{h}}(\hat{\mathbf{q}}_k)$. Again, the vectors $\mathbf{f}_k$ and $\mathbf{h}_k$ are merged into a matrix $\hat{\mathbf{f}} = [\hat{\mathbf{f}}_1, \ldots, \hat{\mathbf{f}}_N]^{\mathrm{T}}$ and $\hat{\mathbf{h}} = [\hat{\mathbf{h}}_1, \ldots, \hat{\mathbf{h}}_N]^{\mathrm{T}}$, respectively. Then, the discrete Fourier transform with real coefficients

$$\hat{\mathbf{F}} = \boldsymbol{\Lambda}^{\mathrm{T}} \hat{\mathbf{f}}\,, \quad \hat{\mathbf{H}} = \boldsymbol{\Lambda}^{\mathrm{T}} \hat{\mathbf{h}}$$

finally yields an approximation for the Fourier transform of the non-linear terms $\tilde{\mathbf{F}}(\mathbf{Q}, \mathbf{U}) \simeq \hat{\mathbf{F}}$ and $\tilde{\mathbf{H}}(\mathbf{Q}) \simeq \hat{\mathbf{H}}$.

4 Calculation of the steady state response

Now a typical question is to calculate the steady state response of the system Eq. 2 due to a harmonic excitation by the input $\mathbf{u}_S = \mathbf{U}_S^{\mathrm{T}} \mathbf{w}$. In terms of the corresponding envelope model of Eq. 4 this is equivalent to the problem of finding the equilibrium $\mathbf{Q}_S$, $\mathbf{V}_S$ of the system Eq. 4 for the constant input $\mathbf{U}_S$. Thus, the steady state can be calculated by setting the time derivatives at the left hand side of Eq. 4a equal to zero, i.e., solving the matrix-valued algebraic equations

$$\begin{aligned} \mathbf{0} &= \mathbf{V}_S^{\mathrm{T}} - \mathbf{Q}_S^{\mathrm{T}} \boldsymbol{\Omega}\,, \\ \mathbf{0} &= -\tilde{\mathbf{K}}(\xi)\, \mathbf{Q}_S^{\mathrm{T}} - \tilde{\mathbf{D}}(\Omega)\, \mathbf{V}_S^{\mathrm{T}} - \tilde{\mathbf{F}}^{\mathrm{T}}(\mathbf{Q}_S, \mathbf{U}_S) - \mathbf{V}_S^{\mathrm{T}} \boldsymbol{\Omega}\,. \end{aligned} \tag{5}$$

In the following it is assumed that the system is excited by the harmonic drive voltage $u_D = U_{D,0} + U_{D,C} \cos(\omega t)$ at the eigenfrequency of the primary mode $\omega = \omega_2$. Furthermore, let us assume that a constant voltage $u_{C,j} = U_{T,0}$, $j = 1, \ldots, m-1$ is applied to the parallel plate actuators. The dimension of the Fourier basis is chosen as $r = 1$ and thus the Fourier coefficient matrix of the input voltages according to Eq. 3 can then be written in the form

$$\mathbf{U}_S = \begin{bmatrix} U_{D,0} & U_{T,0} & \ldots & U_{T,0} \\ 0 & 0 & \ldots & 0 \\ U_{D,C} & 0 & \ldots & 0 \end{bmatrix}.$$

If no external angular rate $\boldsymbol{\Omega}$ is applied to the gyroscope and no mechanical unbalance is present, i.e. $\xi = 0$, the primary mode is fully decoupled from the residual system. In this case the primary mode turns out to behave like a weakly damped second order system that is harmonically excited close to the resonance frequency, thus yielding a large Fourier coefficient $Q_{2,S}$ while the Fourier coefficient $Q_{2,C}$ is vanishing. This effect is exploited within the control design of the primary mode in order to achieve the maximum sensitivity. In general, however, in steady state the system responds to a constant external angular rate $\boldsymbol{\Omega}$ and/or a constant side wall angle ξ in the form

$$\mathbf{Q}_S = \begin{bmatrix} Q_{1,0} & Q_{2,0} & Q_{3,0} & Q_{4,0} & 0 & 0 & Q_{7,0} & Q_{8,0} \\ 0 & Q_{2,S} & Q_{3,S} & 0 & 0 & 0 & Q_{7,S} & 0 \\ 0 & Q_{2,C} & Q_{3,C} & 0 & 0 & 0 & Q_{7,C} & 0 \end{bmatrix},$$

$$\mathbf{Y}_S = \begin{bmatrix} Y_{P,0} & Y_{S,0} \\ Y_{P,S} & Y_{S,S} \\ Y_{P,C} & Y_{S,C} \end{bmatrix}.$$

The only harmonically excited modes are the 2nd and 3rd eigenmodes (primary and secondary mode) as well as the 7th eigenmode. All other modes are either not or only stationarily excited. The only relevant output signals are the harmonic components as due to the high-pass characteristics of the charge amplifiers the dc-components $Y_{P,0}$ and $Y_{S,0}$ are suppressed in the stationary output signal.

In the following the normal operation of the gyroscope shall be investigated in terms of the response to an external angular rate Ω and to a mechanical unbalance due to a side wall angle ξ. For the subsequent numerical calculations a discretization of $N = 10$ for the approximation of the Fourier transforms of the non-linear terms is chosen. The parallel plate actuators are supplied by the constant voltage $U_{T,0} = 9\,\mathrm{V}$. Now, the steady state response of the gyroscope is calculated (a) due to an external angular rate Ω and (b) due to a side wall angle ξ. Figure 2 illustrates the corresponding Fourier coefficients of the output signal $Y_{S,S}$ and $Y_{S,C}$ normalized to the response at $\Omega = 100\,^\circ/s$. Thereby, the range of the side wall angle ξ in Fig. 2(b) is chosen such that the normalized steady state response of the coefficient $Y_{S,S}$ for $\pm\xi_{100}$ is ∓ 1. Now it can be seen from Fig. 2(a) and 2(b) that within the plotted range the coefficients $Y_{S,C}$ and $Y_{S,S}$ are varying linearly with the angular rate and the side wall angle, respectively. The associated phasor diagram of the two coefficients $Y_{S,C}$ and $Y_{S,S}$, see Fig. 2(c), reveals a phase shift of -90° between the output signal due to the angular rate Ω and the output signal due to the side wall angle ξ. This gives rise to the definition of the mechanical unbalance $\Gamma_M = \Gamma_M' \xi$ such that the magnitude $Y_{S,A} = \sqrt{Y_{S,S}^2 + Y_{S,C}^2}$ of the output signal y_S due to an external angular rate of $1\,^\circ/\mathrm{s}$ and due to a mechanical unbalance of $1\,^\circ/\mathrm{s}$ are equivalent. Furthermore, it can be observed that the unwanted unbalance signal can be separated from the angular rate signal by a proper demodulation of the output voltage y_S with two orthogonal reference signals. For a detailed treatise on the unbalance effects of micro electromechanical gyroscopes, see, e.g., Günthner et al (2005). A typical steady state application for the envelope model is the dimensioning of the capacitive actuators for the unbalance compensation and the trimming of the secondary resonance frequency as it has been published by Egretzberger and Kugi (2009).

5 Simulation of the transient response

The verification of the dynamic behavior of the capacitive gyroscope requires transient numerical simulations. For this purpose, the mathematical model Eq. 2 and the corresponding envelope model Eq. 4 are implemented in the simulation environment SIMULINK.

Let us consider a capacitive gyroscope without unbalance in the normal mode of operation as described in Sect. 4

Pre-print version of the article: M. Egretzberger and A. Kugi, "A dynamical envelope model for vibratory gyroscopes", *Microsystem Technologies*, vol. 16, pp. 777–786, 2010. DOI: 10.1007/s00542-009-0979-y
The content of this pre-print version is identical to the published paper but without the publisher's final layout or copy editing.

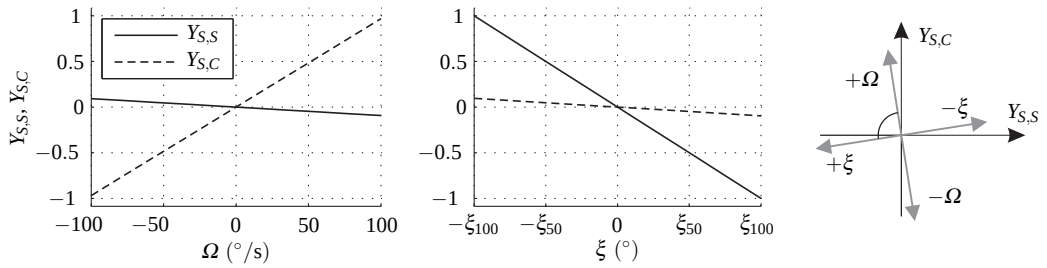

(a) response to external angular rate (b) response to side wall angle (c) phasor diagram

Fig. 2 Steady state response of the system in terms of the Fourier coefficients $Y_{S,S}$ and $Y_{S,C}$ normalized to the response at $\Omega = 100\,^\circ/s$ (a) due to an external angular rate Ω and (b) due to a side wall angle ξ with the appropriate phasor diagram (c).

again with the constant voltage $U_{T,0} = 9\,\mathrm{V}$ applied to the parallel plate actuators. Starting from the initial condition given by the steady state for $\Omega = 0\,^\circ/s$ the transient response to an angular rate step of $100\,^\circ/s$ is simulated.

Figure 3 illustrates the corresponding transient response of the gyroscope in terms of the normalized "fast" output signal y_S and the corresponding "envelope", i.e., the magnitude $Y_{S,A}$. A decaying oscillation with a frequency equivalent to the difference between the primary and secondary eigenfrequency can be observed in the transient response of the envelope $Y_{S,A}$ in Figure 3(a). The close-up view in Figure 3(b), however, reveals that $Y_{S,A}$ additionally contains a small high frequent periodic component which does not contribute to the actual envelope of the original output signal y_S. The elimination of this unwanted high frequency component will be part of the further model simplifications in the following section.

6 Simplified envelope model

Depending on the geometric design of the gyroscope a number of simplifications can be made by applying certain suitable assumptions. If small displacements are assumed for the specific sensor design as depicted in Fig. 1 and the coupling from the primary and secondary mode to the residual modes is neglected the system of Eq. 2 can be reduced to a two-modes model comprising the 2nd and 3rd eigenmodes, i.e., $\mathbf{q} = [q_2, q_3]^\mathrm{T}$. The mechanical stiffness matrix $\tilde{\mathbf{K}}(\xi) = \tilde{\mathbf{K}}_M(\xi)$ and the damping and Coriolis matrix $\tilde{\mathbf{D}}(\Omega)$ can then be written in the form

$$\tilde{\mathbf{K}}_M = \begin{bmatrix} k_{2,M} & \xi\, k_{23,M} \\ \xi\, k_{32,M} & k_{3,M} \end{bmatrix}, \quad \tilde{\mathbf{D}} = \begin{bmatrix} d_2 & \Omega\, c_{23} \\ -\Omega\, c_{32} & d_3 \end{bmatrix}.$$

Furthermore, assuming slowly varying input voltages $u_{C,j}$, $j = 1, \ldots, m-1$ and a harmonically oscillating drive voltage $u_D = U_{D,0} + U_{D,C}\cos(\omega t)$, the non-linear input term $\tilde{\mathbf{f}}$ can be written in the form $\tilde{\mathbf{f}}(\mathbf{q}, \mathbf{u}) = \tilde{\mathbf{K}}_C(u_{C,j})\,\mathbf{q} + \tilde{\mathbf{b}}\,u_D^2$. In general the input voltages $u_{C,j}$ influence both the cross coupling between the primary and secondary mode as well as the secondary resonance frequency. However, in many cases it is possible to find suitable input quantities $\tilde{U}_{T,0}$ and $\tilde{U}_{C,0}$ such that the compensation input $\tilde{U}_{C,0}$ allows for tuning the cross coupling between the primary and the secondary mode while the trimming input $\tilde{U}_{T,0}$ is solely influencing the secondary resonance frequency. Then, the electrostatic stiffness matrix can be written in the form, see, e.g., Ayazi et al (2008),

$$\tilde{\mathbf{K}}_C = \begin{bmatrix} 0 & 0 \\ k_{32,C}(\tilde{U}_{C,0}) & k_{3,T}(\tilde{U}_{T,0}) + k_{3,RO}\,u_{RO}^2 \end{bmatrix}.$$

Furthermore, the input vector takes the form $\tilde{\mathbf{b}} = [b_2, 0]^\mathrm{T}$ and the non-linear output term $\tilde{\mathbf{h}}$ reads as $\tilde{\mathbf{h}}(\mathbf{q}) = \tilde{\mathbf{C}}\,\mathbf{q}$ with the matrix $\tilde{\mathbf{C}} = \mathrm{diag}(c_2, c_3)$. Now, the simplified two-modes model is given by

$$\frac{\mathrm{d}}{\mathrm{d}t}\begin{bmatrix}\mathbf{q}\\ \mathbf{v}\end{bmatrix} = \underbrace{\begin{bmatrix}\mathbf{0} & \mathbf{I}\\ -\tilde{\mathbf{K}}_M - \tilde{\mathbf{K}}_C & -\tilde{\mathbf{D}}\end{bmatrix}}_{\tilde{\mathbf{A}}(\Omega, \xi, \tilde{U}_{T,0}, \tilde{U}_{C,0})}\begin{bmatrix}\mathbf{q}\\ \mathbf{v}\end{bmatrix} - \begin{bmatrix}\mathbf{0}\\ \tilde{\mathbf{b}}\end{bmatrix} u_D^2 \tag{6a}$$

with the output

$$\mathbf{y} = \tilde{\mathbf{C}}\,\mathbf{q}\,. \tag{6b}$$

For the corresponding envelope model of the system Eq. 6 the dimension of the Fourier basis is chosen as $r = 1$ and the coupling from the 0-subsystem (dc-component) to the *S-C*-subsystem (sine and cosine component) is neglected. If the states, i.e., the Fourier coefficients of the primary and secondary mode, are merged to the vector

$$\mathbf{x}_E = \left[Q_{2,S}, Q_{2,C}, Q_{3,S}, Q_{3,C}, V_{2,S}, V_{2,C}, V_{3,S}, V_{3,C}\right]^\mathrm{T}$$

together with the input and output vectors

$$\mathbf{u}_E = \left[0, \tilde{U}_{D,C}\right]^\mathrm{T}, \quad \tilde{U}_{D,C} = 2U_{D,0}U_{D,C}\,,$$

$$\mathbf{y}_E = \left[Y_{P,S}, Y_{P,C}, Y_{S,S}, Y_{S,C}\right]^\mathrm{T}$$

the corresponding envelope model of Eq. 6 can be rewritten in the form

$$\dot{\mathbf{x}}_E = \mathbf{A}_E(\Omega, \xi, \tilde{U}_{T,0}, \tilde{U}_{C,0})\,\mathbf{x}_E + \mathbf{B}_E\,\mathbf{u}_E \tag{7a}$$

$$\mathbf{y}_E = \mathbf{C}_E\,\mathbf{x}_E \tag{7b}$$

Pre-print version of the article: M. Egretzberger and A. Kugi, "A dynamical envelope model for vibratory gyroscopes", *Microsystem Technologies*, vol. 16, pp. 777–786, 2010. DOI: 10.1007/s00542-009-0979-y

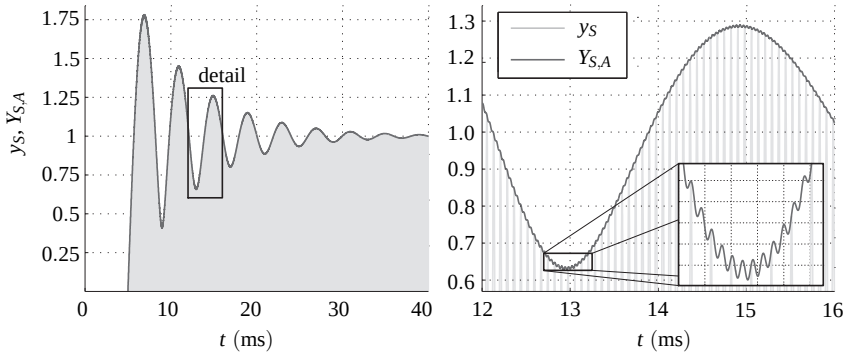

(a) Time-frame of relevant transient effect (b) Close-up (detail)

Fig. 3 Transient response of the system to an input step of the angular rate Ω in terms of the upper half wave of the normalized output y_S and the corresponding envelope $Y_{S,A}$, (a) in a time-frame showing the relevant transient effect and (b) in a close-up view.

with the dynamic matrix

$$\mathbf{A}_E = \begin{bmatrix} 0 & \omega & 0 & 0 & 1 & 0 & 0 & 0 \\ -\omega & 0 & 0 & 0 & 0 & 1 & 0 & 0 \\ 0 & 0 & 0 & \omega & 0 & 0 & 1 & 0 \\ 0 & 0 & -\omega & 0 & 0 & 0 & 0 & 1 \\ -k_2 & 0 & -k_{23} & 0 & -d_2 & \omega & -\Omega c_{23} & 0 \\ 0 & -k_2 & 0 & -k_{23} & -\omega & -d_2 & 0 & -\Omega c_{23} \\ -k_{32} & 0 & -k_3 & 0 & \Omega c_{32} & 0 & -d_3 & \omega \\ 0 & -k_{32} & 0 & -k_3 & 0 & \Omega c_{32} & -\omega & -d_3 \end{bmatrix}$$

and the input and output matrices $\mathbf{B}_E = [\mathbf{0}, \mathbf{B}_{E,2}]^{\mathrm{T}}$ and $\mathbf{C}_E = [\mathbf{C}_{E,1}, \mathbf{0}]$ with the block matrices $\mathbf{B}_{E,2} = -\mathrm{diag}\,(b_2, b_2, 0, 0)$ and $\mathbf{C}_{E,1} = \mathrm{diag}\,(c_2, c_2, c_3, c_3)$, respectively. Thereby, the stiffness parameters are given in the form

$$k_2 = k_{2,M}\,, \qquad k_3 = k_{3,M} + k_{3,T}\left(\tilde{U}_{T,0}\right) + k_{3,RO}\,u_{RO}^2\,,$$
$$k_{23} = \xi\, k_{23,M}\,, \qquad k_{32} = \xi\, k_{32,M} + k_{32,C}\left(\tilde{U}_{C,0}\right)\,.$$

Now, the complex quantities $\lambda_j = \alpha_j \pm \mathrm{i}\,\omega_j$ with

$$\alpha_j = -\frac{1}{2}\,d_j \;\text{ and }\; \omega_j = \frac{1}{2}\sqrt{4k_j - d_j^2}\,, \quad j = 2,3\,, \tag{8}$$

denote the solutions of the relation

$$\det\left(\tilde{\mathbf{A}}\left(0,0,\tilde{U}_{T,0},0\right) - \lambda\,\mathbf{I}\right) = 0\,,$$

i.e., the eigenvalues of the decoupled two modes systems Eq. 6 for a constant trimming input $\tilde{U}_{T,0}$. Thereby, α_j and ω_j are the damping coefficient and the eigenfrequency of the eigenmode q_j, respectively. The eigenvalues of the corresponding simplified envelope system Eq. 7, however, are calculated as the solutions for λ_E of the relation

$$\det\left(\mathbf{A}_E\left(0,0,\tilde{U}_{T,0},0\right) - \lambda_E\,\mathbf{I}\right) = 0$$

and can be written in the form $\lambda_{E,j} = \alpha_j \pm \mathrm{i}\,\omega_{E,j}$ with

$$\omega_{E,j} = \omega_j \pm \omega\,, \quad j = 2,3\,. \tag{9}$$

Hence, it can be concluded that the eigenvalues of the original system (Eq. 6) and of the corresponding envelope model (Eq. 7) have the identical damping coefficients α_j, while the eigenfrequencies alter with the phase velocity ω resulting in "slow" eigenfrequencies $\omega_j - \omega$ and "fast" eigenfrequencies $\omega_j + \omega$. Thus, the decoupled envelope model (Eq. 7) can be separated into a "fast" and a "slow" subsystem by means of the state transformation $\mathbf{x}_E = \mathbf{V}\,\mathbf{z}_E$ with the regular matrix $\mathbf{V}$ in the so-called real Jordan form, see, e.g., Reid (1983),

$$\dot{\mathbf{z}}_E = \tilde{\mathbf{A}}_E\,\mathbf{z}_E + \tilde{\mathbf{B}}_E\,\mathbf{u}_E\,, \tag{10a}$$
$$\mathbf{y}_E = \tilde{\mathbf{C}}_E\,\mathbf{z}_E \tag{10b}$$

with the matrices $\tilde{\mathbf{A}}_E = \mathbf{V}^{-1}\mathbf{A}_E\mathbf{V}$, $\tilde{\mathbf{B}}_E = \mathbf{V}^{-1}\mathbf{B}_E$ and $\tilde{\mathbf{C}}_E = \mathbf{C}_E\mathbf{V}$. The decoupled system in Jordan form with the state vector $\mathbf{z}_E = [\mathbf{z}_{E,1}^{\mathrm{T}}, \mathbf{z}_{E,2}^{\mathrm{T}}]^{\mathrm{T}}$ possesses the dynamic matrix

$$\tilde{\mathbf{A}}_E\left(0,0,\tilde{U}_{T,0},0\right) = \begin{bmatrix} \tilde{\mathbf{A}}_{E,11} & \mathbf{0} \\ \mathbf{0} & \tilde{\mathbf{A}}_{E,22} \end{bmatrix}$$

composed of the block matrices

$$\tilde{\mathbf{A}}_{E,11(22)} = \begin{bmatrix} \alpha_2 & \omega_2 \overset{(+)}{(-)} \omega & 0 & 0 \\ -\omega_2 \overset{(-)}{(+)} \omega & \alpha_2 & 0 & 0 \\ 0 & 0 & \alpha_3 & \omega_3 \overset{(+)}{(-)} \omega \\ 0 & 0 & -\omega_3 \overset{(-)}{(+)} \omega & \alpha_3 \end{bmatrix}.$$

Henceforth, the subsystem with the state vector $\mathbf{z}_{E,1}$ and the dynamic matrix $\tilde{\mathbf{A}}_{E,11}$ will be referred to as the "slow" subsystem and the subsystem with the state vector $\mathbf{z}_{E,2}$ and the dynamic matrix $\tilde{\mathbf{A}}_{E,22}$ as the "fast" subsystem. Since it is desired for the normal operation of the gyroscope to harmonically excite the system close to its resonance frequencies it can be assumed that there exist small parameters $\varepsilon_j \ll 1$ with the property

$$(\omega_j + \omega)\,\varepsilon_j = \omega_j - \omega\,, \quad j = 2,3\,.$$

Thus, the fast subsystem can be eliminated by applying the singular perturbation theory, see, e.g., Kokotovic et al (1986),

Pre-print version of the article: M. Egretzberger and A. Kugi, "A dynamical envelope model for vibratory gyroscopes", *Microsystem Technologies*, vol. 16, pp. 777–786, 2010. DOI: 10.1007/s00542-009-0979-y

with ε_2 and ε_3 as the singular perturbation parameters yielding $z_{E,2} = 0$ in the quasi-static case.

In general, however, the system given by Eq. 10 is coupled by the side-wall angle ξ, the compensation input $\tilde{U}_{C,0}$ and the external angular rate Ω. Nevertheless, it can be assumed that the gyroscopes under consideration are weakly coupled systems and the quasi-static treatment of the fast subsystem in the sense of the singular perturbation theory is still justified. Then, the remaining slow subsystem can be transformed back to the original coordinates by means of the inverse state transformation $\mathbf{z}_{E,1} = \mathbf{V}_{11}^{-1}\mathbf{x}_R$ with $\mathbf{V}_{11}$ denoting the upper left block matrix of $\mathbf{V}$. The inverse transformation applied to the residual slow system finally yields the reduced and simplified envelope model

$$\dot{\mathbf{x}}_R = \mathbf{A}_R\mathbf{x}_R + \mathbf{B}_R\mathbf{u}_E \ , \tag{11a}$$

$$\mathbf{y}_E = \mathbf{C}_R\mathbf{x}_R \tag{11b}$$

with the reduced state vector

$$\mathbf{x}_R = [Q_{2,S}, Q_{2,C}, Q_{3,S}, Q_{3,C}]^{\mathrm{T}} \ ,$$

the dynamic matrix

$$\mathbf{A}_R = \mathbf{V}_{11}\tilde{\mathbf{A}}_{E,11}\mathbf{V}_{11}^{-1} = \begin{bmatrix} \alpha_2 & \omega-\omega_2 & -\frac{1}{2}\frac{\omega_3\,\Omega\,c_{23}}{\omega_2} & -\frac{1}{2}\frac{k_{23}}{\omega_2} \\ -\omega+\omega_2 & \alpha_2 & \frac{1}{2}\frac{k_{23}}{\omega_2} & -\frac{1}{2}\frac{\omega_3\,\Omega\,c_{23}}{\omega_2} \\ \frac{1}{2}\frac{\omega_2\,\Omega\,c_{32}}{\omega_3} & -\frac{1}{2}\frac{k_{32}}{\omega_3} & \alpha_3 & \omega-\omega_3 \\ \frac{1}{2}\frac{k_{32}}{\omega_3} & \frac{1}{2}\frac{\omega_2\,\Omega\,c_{32}}{\omega_3} & -\omega+\omega_3 & \alpha_3 \end{bmatrix} ,$$

the input matrix

$$\mathbf{B}_R = \mathbf{V}_{11}\tilde{\mathbf{B}}_{E,1} = \begin{bmatrix} 0 & -\frac{1}{2}\frac{b_2}{\omega_2} \\ \frac{1}{2}\frac{b_2}{\omega_2} & 0 \\ 0 & 0 \\ 0 & 0 \end{bmatrix}$$

and the output matrix

$$\mathbf{C}_R = \mathbf{C}_{E,1}\mathbf{V}_{11}^{-1} = \mathrm{diag}\,(c_2, c_2, c_3, c_3) \ .$$

Typically, the amplitudes of the primary mode excited by the input $\tilde{U}_{D,C}$ are several orders of magnitude larger than the amplitudes of the secondary mode excited by the weak coupling to the primary mode due to the angular rate Ω and/or the side wall angle ξ. Hence, it is reasonable to assume that the coupling from the secondary to the primary mode is considerably small. For the control of the primary mode it therefore suffices to consider the subsystem

$$\frac{\mathrm{d}}{\mathrm{d}t}\begin{bmatrix} Q_{2,S} \\ Q_{2,C} \end{bmatrix} = \begin{bmatrix} \alpha_2 & \omega-\omega_2 \\ -\omega+\omega_2 & \alpha_2 \end{bmatrix}\begin{bmatrix} Q_{2,S} \\ Q_{2,C} \end{bmatrix} - \begin{bmatrix} \beta_2 \\ 0 \end{bmatrix}\tilde{U}_{D,C} \tag{12a}$$

with the output

$$\begin{bmatrix} Y_{P,S} \\ Y_{P,C} \end{bmatrix} = \begin{bmatrix} c_2 & 0 \\ 0 & c_2 \end{bmatrix}\begin{bmatrix} Q_{2,S} \\ Q_{2,C} \end{bmatrix} \tag{12b}$$

and the input coefficient

$$\beta_2 = \frac{1}{2}\frac{b_2}{\omega_2} \ .$$

For the control design it is advantageous at this stage to introduce an output transformation to polar coordinates in the form

$$Y_{P,A} = \sqrt{Y_{P,S}^2 + Y_{P,C}^2} \ , \quad Y_{P,\varphi} = \arctan\left(\frac{Y_{P,S}}{Y_{P,C}}\right)$$

with the amplitude $Y_{P,A}$ and the phase $Y_{P,\varphi}$ of the primary output voltage. In steady state the amplitude and phase of the primary output voltage read as

$$Y_{P,A} = \frac{\beta_2\,c_2\,\tilde{U}_{D,C}}{\sqrt{\alpha_2^2 + (\omega-\omega_2)^2}} \ , \quad Y_{P,\varphi} = \arctan\left(\frac{\alpha_2}{\omega-\omega_2}\right) \ .$$

The maximum amplitude $Y_{P,A}$ in steady state is observed for the angular velocity $\omega = \omega_2$ where at the same time for $\alpha_2 < 0$ the phase is $Y_{P,\varphi} = -\pi/2$. Hence, the first two tasks concerning the control of the primary mode can be formulated as follows. The output phase $Y_{P,\varphi}$ is controlled to $-\pi/2$ and the output amplitude $Y_{P,A}$ is controlled to a predefined constant value $Y_{P,des}$.

For the following let us assume that the primary mode is ideally controlled with $Y_{P,A} = Y_{P,des}$ and $Y_{P,\varphi} = -\pi/2$ yielding the steady state $Q_{2,S} = Y_{P,des}/c_2$ and $Q_{2,C} = 0$. Now, the idea of the mechanical unbalance introduced in Sect. 4 can be picked up in the context of the simplified two modes envelope model. For this purpose, the mechanical unbalance Γ_M and the unbalance compensation parameter Γ_C are introduced in the form

$$\Gamma_M = \frac{k_{32,M}}{\omega_2\,c_{32}}\,\xi \ , \quad \Gamma_C = \frac{k_{32,C}\,(\tilde{U}_{C,0})}{\omega_2\,c_{32}} \ . \tag{13}$$

Substituting the ideally controlled steady state for the primary mode $Q_{2,S} = Y_{P,des}/c_2$, $Q_{2,C} = 0$ and $\omega = \omega_2$ together with the unbalance parameters from Eq. 13 yields the residual differential equations for the secondary mode in the form

$$\frac{\mathrm{d}}{\mathrm{d}t}\begin{bmatrix} Q_{3,S} \\ Q_{3,C} \end{bmatrix} = \begin{bmatrix} \alpha_3 & \omega_2-\omega_3 \\ -\omega_2+\omega_3 & \alpha_3 \end{bmatrix}\begin{bmatrix} Q_{3,S} \\ Q_{3,C} \end{bmatrix} + \begin{bmatrix} \beta_{32}\,\Omega \\ \beta_{32}\,(\Gamma_M+\Gamma_C) \end{bmatrix} \tag{14a}$$

with the output

$$\begin{bmatrix} Y_{S,S} \\ Y_{S,C} \end{bmatrix} = \begin{bmatrix} c_3 & 0 \\ 0 & c_3 \end{bmatrix}\begin{bmatrix} Q_{3,S} \\ Q_{3,C} \end{bmatrix} \tag{14b}$$

Pre-print version of the article: M. Egretzberger and A. Kugi, "A dynamical envelope model for vibratory gyroscopes", *Microsystem Technologies*, vol. 16, pp. 777–786, 2010. DOI: 10.1007/s00542-009-0979-y

and the coupling parameter

$$\beta_{32} = \frac{1}{2}\frac{\omega_2}{\omega_3}\frac{c_{32}\,Y_{P,des}}{c_2} \ .$$

In order to separate the response due to the external angular rate from the response due to the mechanical unbalance the output transformation

$$\begin{bmatrix} Z_{S,R} \\ Z_{S,Q} \end{bmatrix} = \begin{bmatrix} \sin(\phi) & \cos(\phi) \\ \cos(\phi) & -\sin(\phi) \end{bmatrix} \begin{bmatrix} Y_{S,S} \\ Y_{S,C} \end{bmatrix} \ , \qquad \phi = \arctan\left(\frac{\alpha_3}{\omega_2 - \omega_3}\right) \tag{15}$$

is performed. Then, the steady state of the system Eq. 14 with the subsequent output transformation from Eq. 15 yields the Fourier coefficients of the transformed output signals

$$Z_{S,R} = -S\,\Omega \ , \quad Z_{S,Q} = S\,(\Gamma_M + \Gamma_C) \tag{16}$$

with the sensitivity

$$S = \frac{\beta_{32}\,c_3}{\sqrt{\alpha_3^2 + (\omega_2 - \omega_3)^2}} \ . \tag{17}$$

Now, the system Eq. 14 is stationary decoupled and the components $Z_{S,R}$ and $Z_{S,Q}$ are denoted as the angular rate signal and the quadrature signal, respectively. It can be seen from Eq. 16 that the mechanical unbalance is exactly compensated for $\Gamma_C = -\Gamma_M$, which is achieved by controlling the quadrature signal $Z_{S,Q}$ to zero. The angular rate signal $Z_{S,R}$ serves as the measurement output of the gyroscope.

7 Summary

The presented work provides a novel approach for the modeling, simulation and optimization of oscillating micro electromechanical devices in particular of vibratory MEMS gyroscopes. The methodology was exemplarily demonstrated for a capacitive gyroscope. The advantages of the proposed approach were outlined for steady state as well as transient simulations. Moreover, special emphasis was laid on the derivation of a simplified two modes envelope model. The principle of operation and the essential control tasks of vibratory gyroscopes were discussed on basis of this simplified envelope model.

Acknowledgements This work was funded by the German BMBF as part of the EURIPIDES project RESTLES (project no. V3EUR015).

References

Alper S, Akin T (2001) A symmetric surface micromachined gyroscope with decoupled oscillation modes. In: The 11th international conference on solid-state sensors and actuators, Munich, pp 456–459

Ayazi F, Zaman MF, Sharma A (2008) Vibrating gyroscopes. In: Gianchandani YB, Tabata O, Zappe H (eds) Comprehensive Microsystems, vol 2, Elsevier, Amsterdam, The Netherlands, pp 181–208

Bernstein J, Cho S, King AT, Kourepenis A, Maciel P, Weinberg M (1993) A micromachincd comb-drive tuning fork rate gyroscopce. In: Proceedings MEMS, pp 143–148

Bhave SA, Seeger JI, Jiang X, Boser BE, Howe RT, Yasaitis J (2003) An integrated vertical-drive, in-plane-sense microgyroscope. In: Digest of technical papers of the 12th international conference on solid-state sensors, sctuators and microsystems, Boston, pp 171–174

Braxmaier M, Gaißer A, Link T, Schumacher A, Simon I, Frech J, Sandmaier H, Lang W (2003) Cross-coupling of the oscillation modes of vibratory gyroscopes. In: Digest of technical papers of the 12th international conference on solid-state sensors, actuators and microsystems, Boston, pp 167–170

Caliskan VA, Verghese GC, Stankovic AM (1996) Multifrequency averaging of DC/DC converters. In: IEEE workshop on computers in power electronics, Portland, pp 113–119

Egretzberger M, Kugi A (2009) An envelope model to describe the sensor dynamics of vibratory gyroscopes. In: Proceedings of the SPIE, smart sensors, actuators and MEMS IV, Dresden, vol 7362

Feldman P, Roychowdhury J (1996) Computation of circuit waveform envelopes using an effcient, matrix-decomposed harmonic balance algorithm. In: Digest of technical papers of the ICCAD, IEEE/ACM international conference, San Jose, pp 295–300

Günthner S (2006) Entwurf und Charakterisierung von mikromechanischen Drehratensensoren in Silizium. In: Aktuelle Berichte aus der Mikrosystemtechnik, Shaker Verlag, Aachen

Günthner S, Egretzberger M, Kugi A, Kapser K, Hartmann B, Schmid U, Seidel H (2005) Compensation of parasitic effects for a silicon tuning fork gyroscope. IEEE Sens J 6:596–604

Juneau T, Pisano AP, Smith JH (1997) Dual axis operation of a micromachined rate gyroscope. In: The 9th international conference on solid-state sensors, actuators and microsystems, Chicago, vol 2, pp 883–886

Kanso E, Szeri AJ, Pisano AP (2004) Cross-coupling errors of micromachined gyroscopes. J Micromech Syst 13:323–331

Pre-print version of the article: M. Egretzberger and A. Kugi, "A dynamical envelope model for vibratory gyroscopes", *Microsystem Technologies*, vol. 16, pp. 777–786, 2010. DOI: 10.1007/s00542-009-0979-y

Kokotovic P, Khalil HK, O'Reilly J (1986) Singular Perturbation Methods in Control: Analysis and Design. Academic Press Inc., Philadelphia

Kuisma H, Ryhänen T, Lahdenperä J, Punkka E, Routsalainen S, Silanpää T, Seppä H (1997) A bulk micromachined angular rate sensor. In: The 9th international conference on solid-state sensors, actuators and microsystems, Chicago, pp 875–878

Loveday PW, Rogers CA (2002) The influence of control system design on the performance of vibratory gyroscopes. J Sound Vib 255:417–432

Maenaka K, Fujita T, Konishi Y, Maeda M (1996) Analysis of a highly sensitive silicon gyroscope with cantilever beam as vibrating mass. Sens Actuators A 54:568–573

Mair F, Egretzberger M, Kugi A (2009) A tool for the automatic modeling of capacitive MEMS gyroscopes. In: Proceedings of the 6th Vienna international conference on mathematical modelling, Vienna, pp 2228–2235

Merz P, Pilz W, Senger F, Reimer K, Grouchko M, Pandhumsoporn T, Bosch W, Cofer A, Lassig S (2007) Impact of Si DRIE on vibratory MEMS gyroscope performance. In: The 14th international conference on solid-state sensors, actuators and microsystems, Lyon, pp 1187–1190

Piyabongkarn D, Rajamani R, Greminger M (2005) The development of a MEMS gyroscope for absolute angle measurement. IEEE Trans Control Syst Technol 13:185–195

Reid JG (1983) Linear System Fundamentals. McGraw-Hill, New York

Sassen S, Voss R, Schalk J, Stenzel E, Gleissner T, Grünberger R, Neubauer F, Ficker W, Kupke W, Bauer K, Rose M (2000) Tuning fork silicon angular rate sensor with enhanced performance for automotive applications. Sens Actuators A 83:80–84

Seeger JI, Boser BE (2003) Charge control of parallel-plate, electrostatic actuators and the tip-in instability. J Micromech Syst 12:656–671

Seshia AA, Howe RT, Montaguet S (2002) An integrated microelectromechanical resonant output gyroscope. In: The 15th IEEE international conference on micro electro mechanical systems, Las Vegas, pp 722–726

Pre-print version of the article: M. Egretzberger and A. Kugi, "A dynamical envelope model for vibratory gyroscopes", *Microsystem Technologies*, vol. 16, pp. 777–786, 2010. DOI: 10.1007/s00542-009-0979-y